Electrochemical Properties of Silver Nanoparticles in Mesoporous Silica and Titania Films: Specific Behavior of Titania Composite

Fernand Chassagneux, Nelly Couzon, Christophe Place, Mathieu Maillard, Arnaud Brioude, Laurence Bois

Electrochemical Properties of Silver Nanoparticles in Mesoporous Silica and Titania Films: Specific Behavior of Titania Composite.

Fernand Chassagneux[*,a], Nelly Couzon[a], Christophe Place[b], Mathieu Maillard[a], Arnaud Brioude[a], Laurence Bois*[*,a]*

[a] Laboratoire Multimatériaux et Interfaces, UMR CNRS 5615, Université Claude Bernard Lyon 1, 6, rue Victor Grignard, 69266 Villeurbanne, France.

[b] Laboratoire de Physique de l'ENS Lyon, UMR CNRS 5672, 46, allée d'Italie, F-69364 Lyon cedex07, France.

Corresponding authors:

- Fernand Chassagneux

  Laboratoire Multimatériaux et Interfaces, UMR CNRS 5615, Université Claude Bernard Lyon 1, 6, rue Victor Grignard, 69266 Villeurbanne, France. Email: fernand.chassagneux@univ-lyon1.fr

- Laurence Bois

  Laboratoire Multimatériaux et Interfaces, UMR CNRS 5615, Université Claude Bernard Lyon 1, 6, rue Victor Grignard, 69266 Villeurbanne, France. Email: laurence.bois@univ-lyon1.fr

KEYWORDS. Silver nanoparticles, mesoporous titania, cyclic voltammetry.

ABSTRACT

Electrochemical behavior of silver nanoparticles in mesoporous oxides electrodes is investigated. Mesoporous SiO_2 and TiO_2 films deposited on FTO (Fluorine doped tin oxide) and containing Ag nanoparticles (NPs) are used as electrodes. The study of voltammetric curves (CVs) and the diffusion of Ag^+ ions out of the films highlight the importance of the retention of Ag^+ ions by the TiO_2 films. By varying several factors such as the speed rate or the initial potential, we observe the existence of the two potentials anodic peaks. These are explained by the nature of two silver NPs populations created in two distinct areas in the film and with different size distributions, as shown by Scanning Electron Microscopy (SEM) and Transmission Electron Microscopy (TEM) observations. The size distributions of the two NPs populations allow the position and shape of each of the oxidation peaks in the CVs to be adequately simulated.

Introduction

Metallic nanoparticles have different interesting properties, such as optical, chemical or electrochemical which are size-dependent.[1–10] They are explored in various fields of applications such as catalysis, plasmonic, electrochemical sensing or optical detection.[1,7,11,12] The performance of these nanoparticles depends on their stability. The oxidative dissolution is an important reason of their instability.[3,7,9,13]

After establishing the equations to obtain the variation of the Redox potential of small metal particles as a function of their size, Plieth[14] has described their electrochemical behavior, the negative shift of the equilibrium potential, the negative shift of the point of zero charge (PZC) and the decrease of the work function (W). These observations are in agreement with the results obtained by Henglein *& al*. [15] showing a very high reducing power of silver aggregates consisting of a few atoms. Observed qualitatively,[16] the decrease in standard redox potential with the size of silver NPs was measured by Ivanova *& al*.[17] Brainina *& al* has shown that the dissolution potential of metallic NPs deposited on a support electrode also depends on the nature of this support.[18] Electrochemical stripping processes have been developed for the study of many solids with various electrodes.[19] In this regard,

Chevallier *& al.*[20] and Ward Jones *& al.*[21,22] stressed the importance of the phenomena of diffusion of ionic soluble species resulting from electrooxidation. Toh *& al.*[23] have shown the influence of the reversible or irreversible type of electronic transfer, the coverage rate, the agglomeration and whether the diffusion layers around the NPs are independent or overlapping. Brainina *& al.*[24] proposed mathematical models to explain the influence of NPs size on the characteristics of voltamperometric curves plotted during the abrasion of gold and silver NPs.[13,25] Silver NPs supported on oxide can be used for many applications such as catalysis,[26–33] as Surface Enhanced Raman Spectroscopy (SERS) substrates[34] or as electrochemical sensor.[35,36] The interest of silver NPs and titania films has also been related for their photochromic properties.[37–45] and we have previously described the photoelectrochemical behavior of silver NPs inside mesoporous TiO_2 films.[46,47]

In mesoporous buildings, the phenomena of diffusion of matter in the different gaseous, liquid and solid forms are the subject of numerous studies.[45,48–51] Electrochemical methods, especially those using a "walljet electrode" have made it possible to measure the permeation of mesoporous thin films.[52] For example, an electrochemical study on the molecular transport of various ions and molecules in thin films of silica p6m, $P6_3/mmc$, Pm3n highlight the role of mesostructure isoelectric point (IEP), charge and dimension of the diffusing entity and also of the thickness of the layer deposited on the ITO substrate.[53]

Following these studies, the purpose of this article is to study through electrochemistry the characteristics and stability of two electrodes made of mesoporous oxides films, deposited on FTO, titania and silica, and loaded with silver NPs. To build mesoporous silica and titania films, a sol-gel process and block copolymer self-assembly method has been used.[54,55] Among the numerous methods existing to form silver NPs in mesoporous films,[45,56,46,47] a reduction of silver ions solution by coulometric method have been chosen to control the quantities of silver introduced.[57–60] Using these materials as electrodes, the influence of experimental parameters on voltamperometric curves CV such as the scanning speed and the starting potential are examined. To explain the form and position of the recorded anodic peaks, the results are analyzed in the light of previously published work[13,18–25] and using SEM and TEM observations. The high retention of Ag^+ ions is then demonstrated in mesoporous films of titanium oxide.

Experimental Section

Materials

Poly(ethylene oxide)-poly(propylene oxide)-poly(ethylene oxide) block copolymer, Pluronic P-123 ($(EO)_{20}$-$(PO)_{70}$-$(EO)_{20}$), poly(ethylene oxide)-poly(propylene oxide)-poly(ethylene oxide) block copolymer, Pluronic F-127 ($(EO)_{106}$-$(PO)_{70}$-$(EO)_{106}$), tetrabutylorthotitanate ($Ti(OBu)_4$), silver nitrate ($AgNO_3$), and tetraethoxysilane ($Si(OEt)_4$), were all purchased from Sigma-Aldrich and used as received. The FTO (fluorine-doped tin oxide) substrates (3×3 cm, 600 nm of FTO-deposited by Chemical Vapor Deposition (CVD) on glass) were purchased from Solems.

Mesoporous electrodes

Two electrodes made of the mesoporous oxides TiO_2 and SiO_2 with similar textural characteristics were prepared in order to identify the influence of the chemical nature of the oxide.

TiO_2 mesoporous film and Ag -TiO_2 electrode preparation

The titania sol was prepared by mixing $Ti(OBu)_4$ (3.4 g), ethanol (12 g), hydrochloric acid (HCl, 37%) (3 mL) and a triblock copolymer P-123 (1 g). After stirring for 30 minutes, films were then deposited by a dip-coating method on FTO substrates with a withdrawal speed of 2 $mm.s^{-1}$, at room temperature. The films were aged under ambient conditions (T = 23 °C, RH = 30-40%) for 24 h and then calcined at 350 °C for 2 h, with a heating ramp of 1 $°C.min^{-1}$. These films are about 200 nm thick and have a mesoporous volume equal to 0.25 $cm^3.g^{-1}$, provided by pores of 11 nm average diameter.[61]

In order to form silver NPs inside the porous oxide films, the titania films were immersed in a silver nitrate solution (50 mM). Silver NPs were formed by coulometry by imposing in general on the working electrode constitut-

ed by the mesoporous film deposited on FTO a current of -10 μA for 180 s. The amount of silver introduced corresponds to a load of -1.8 mC. For an electrode surface of 6 cm^2, the coverage rate is then 3.0 $C.m^{-2}$, or $3.1.10^{-5}$ $molAg.m^{-2}$ or $7.8.10^{13}$ $particles.m^{-2}$ considering that the particles are spheres of 20 nm in diameter, as an example of a calculation to fix the ideas. During coulometry, the potential of the working electrode was between about 480 and 510 mV/(AgCl/Ag). This electrode is named Ag-TiO_2.

SiO_2 mesoporous film and Ag -SiO_2 electrode preparation

The silica sol was prepared by mixing $Si(OEt)_4$ (4 g), ethanol (12 g), H_2O acifidied to pH 2 with chlorohydric acid (HCl, 37%) (1.76 g) and F-127 triblock copolymer (1 g). Mesoporous silica films and silver NPs were synthesized by the same method than in titania electrode, to form the electrode named Ag-SiO_2. The morphological characteristics of these films are similar to those of mesoporous titanium oxide films and were determined in the same way. The thickness is equal to 200 nm, the pores have an average diameter of 10 nm. The mesoporous volume of 0.40 $cm^3.g^{-1}$ is however higher.

Non-porous electrodes

To study the influence of porosity on the electrochemical response of silver, two more electrodes were prepared using only silver NPs. Two preparation methods have been used: a coulometry deposition (Ag-FTO), using the same conditions than for TiO_2-Ag and SiO_2-Ag electrodes, and a thermochemical process with a vacuum treatment at 300°C (Ag300-FTO). For that, silver nitrate (160 mg) and F-127 block copolymer (1 g) were dissolved in ethanol (12 g). After stirring for 30 minutes, films were then deposited by a dip-coating method on FTO substrates with a withdrawal speed of 2 $mm.s^{-1}$, at room temperature. The films were aged under ambient conditions (T = 23 °C, RH = 30-40%) for 24 h and then thermally treated under vacuum at 300 °C for 2 h, with a heating ramp of 1 $°C.min^{-1}$. These samples will serve as controls and we will discuss the behavior of these electrodes later.

Characterization

Scanning electron microscopy (SEM) images were obtained using a Zeiss Merlin Compact SEM with an in-lens detector at a low acceleration voltage of 5 kV. Energy dispersive X-ray analysis (EDX) was used to determine the amount of silver within the oxide film. Transmission electron microscopy (TEM) was performed on a JEOL 2100F field emission instrument operating at 200 kV. Particle size distributions were made from the SEM and TEM images using "image J".

All electrochemical measurements were performed using a Voltamaster Potentiostat with a three-electrode cell. The counter electrode consists of a platinum disc with a surface area of 1 cm^2 and the reference electrode is one electrode Ag/AgCl in a KCl 3 M solution with a potential relative to Normal Hydrogen Electrode (NHE) of 0.200 V at 20 °C. The working electrode is the mesoporous oxide film loaded with silver NPs deposited on FTO. The electrochemically active area of the film is 6 cm^2. The voltamperometric (CV) and chronoamperometric (CA) curves were plotted in a molar solution of sodium nitrate used as an electrolyte, at room temperature. The high electrolyte concentration of 1 $mol.L^{-1}$ has been chosen so that the ionic strength would be as constant as possible during the various electrochemical reactions. Open circuit potential (OCP) measurements were performed with the same background salt. This electrolyte with a pH close to 6 avoids the attack of the titanium film and minimizes the dissolution of the silica film that occurs in some more aggressive environments.[62,63] The standard condition of CV was the following: from -0.3V to 1.1V, with a scan speed of 100 $mV.s^{-1}$.

Results and Discussion

CVs plotted between -0.3 and 1.1 V, with electrodes Ag-TiO_2, Ag-SiO_2, Ag-FTO and Ag300-FTO

Most CVs are plotted between -0.3 and 1.1 V/AgCl/Ag. In this wide potential range, the FTO, the mesoporous oxides and the electrolyte remain electrochemically inactive. In the case of Figure 1, five cycles are performed at a speed of 100 $mV.s^{-1}$. The first scan of Ag-TiO_2's CV (Figure 1a) shows two anodic peaks, the first peak, P_1, with a maximum located at 0.32 V and the second, P_2, with a maximum at 0.65 V. For Ag-SiO_2 (Figure 1b), only one main anodic peak is observed with a maximum around 0.65 V, corresponding to P_2. This electrochemical behavior is similar to the one observed for the silver NPs deposited directly on FTO (Figure 1c). The CVs made with

the vacuum treated film Ag-300-FTO are characterized by the absence at the first scan of the first peak around 0.30 V, there is then only one peak whose summit is located at 0.63 V (Figure 1d). During the following scans, the first peak appears only very faintly around 0.40 V. We note that for all electrodes, at the first scan, there is at least one peak whose summit is located a little above 0.60 V under these experimental conditions. This peak disappears from the second cycle. The peak between 0.30 and 0.45 V disappears after a small number of cycles except for the Ag-TiO_2 electrode for which the P_1 peak still has a perceptible intensity after a hundred cycles and evolves slowly towards lower potentials. Two peaks have already been observed, although less spaced: during CVs performed on a vitreous carbon electrodes coated with silver NP of different sizes, in phosphate buffer.[64] The conditions for observing this first oxidation peak P_1 are therefore i) the presence of silver nanoparticles ii) in a mesoporous film iii) consisting of TiO_2.

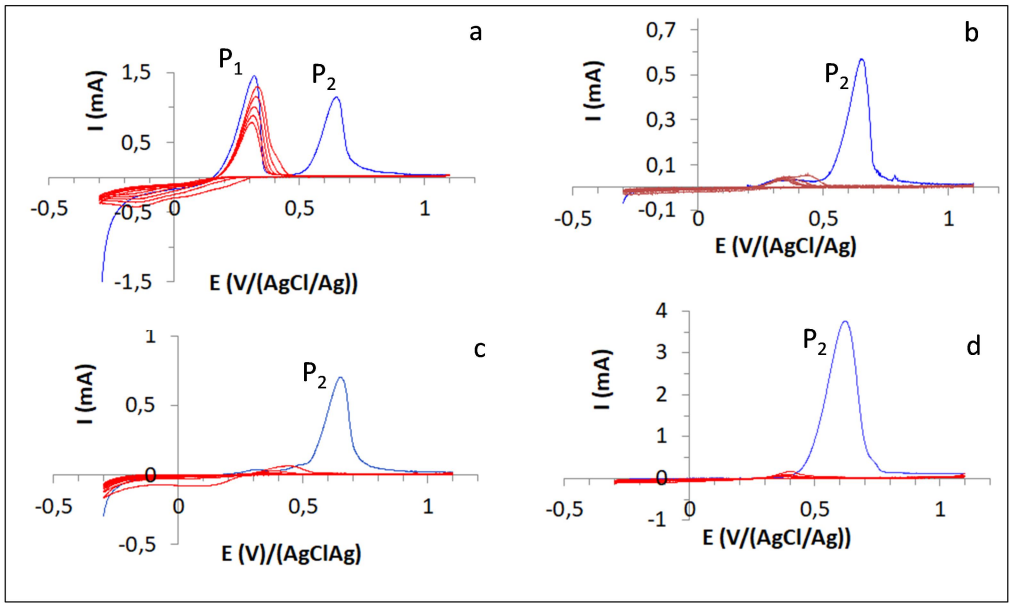

Figure 1: CV performed at a speed of 100 $mV.s^{-1}$, in molar sodium nitrate medium. In blue, first scan between - 300 and 1100 mV. In red, following cycles of different electrodes. (a): Ag-TiO_2. (b): Ag-SiO_2. (c): Ag-FTO. (d): Ag-300- FTO. The two anodic peaks are named P_1, with a maximum located at 0.32 V and P_2, with a maximum at 0.65 V.

The appearance of two distinct P_1 and P_2 peaks, in particular the very intense P_1 peak in the CV of the Ag-TiO_2 electrode, was unexpected. Indeed, the coulometric preparation method should have led to a single type of silver NPs. We then sought to determine the origin of this characteristic, on the one hand by carrying out a precise bal-

ance of the charges exchanged during the CVs and on the other hand by varying the acquisition conditions of the CVs.

Electrochemical balance

The high negative intensity at the start of the CVs of the Ag-TiO_2 electrode (Figure 1a), which is not due to a capacitive current, highlights a significant reduction phenomenon likely to explain the singular behavior of this film. While this negative intensity is important in Ag-TiO_2, there is very little of it in Ag-FTO (Figure 1c) and is practically non-existent in Ag-SiO_2 (Figure 1b) and the vacuum treated film Ag-300-FTO (Figure 1d). Table 1 shows the various charges calculated on the basis of the CVs recorded during the first scan towards the positive potentials. In this table, "$Q_{introduced}$" corresponds to the load introduced by coulometry i.e. -1.8 mC. "$Q_{reduction}$" is the amount of electricity exchanged from the start of the CV (-0.3 V) to the potential where the current becomes positive (about 0.1 V). "$Q_{1\ anodic}$" and "$Q_{2\ anodic}$" are the charges exchanged during the first anodic peak P_1 and during the second anodic peak P_2, respectively. "$Q_{total\ anodic}$" represents the sum " $Q_{1\ anodic}$ " and " $Q_{2\ anodic}$".

Table 1: Load introduced and loads exchanged in the CVs carried out at a speed of 100 $mV.s^{-1}$, during the first scan for the electrodes. $Q_{introduced}$ is the load introduced by coulometry. $Q_{reduction}$ is the load exchanged from -0.3 V to 0.1 V. $Q_{1\ anodic}$ and $Q_{2\ anodic}$ are the loads exchanged in the P_1 and P_2 peaks, respectively. $Q_{total\ anodic}$ is the sum of $Q_{1\ anodic}$ and $Q_{2\ anodic}$.

Electrode	$Q_{introduced}$ (mC)	$Q_{reduction}$ (mC)	$Q_{1\ anodic}$ (mC)	$Q_{2\ anodic}$ (mC)	$Q_{total\ anodic}$ (mC)
Ag-TiO_2	- 1.80	- 1.46	1.44	1.49	2.93
Ag-SiO_2	-1.80	~ - 0.05	0.05	0.83	0.88
Ag-FTO	-1.80	~ - 0.15	~ 0.00	0.70	~ 0.70
Ag300-FTO	*	0.00	0.00	5.95	5.95

* Only the $AgNO_3$/F-127 ratio of 16 w% is known, before heat treatment.

The load balance of positive and negative charges from the CVs sum in Table 1 highlights the particularity of the film TiO_2. We find that the loads exchanged during the CVs of the Ag-TiO_2 electrode are greater than those exchanged in the other electrodes obtained by coulometry. In this voltammetry curve, the charge "$Q_{1\ anodic}$" is of the same order of magnitude as "$Q_{2\ anodic}$" and in absolute value equal as "$Q_{reduction}$". This equality leads us to

consider that the "$Q_{reduction}$" charge comes from the formation of silver NPs from Ag^+ ions present inside the films at the start of the CV. We can hypothesize that these NPs dissolve during the P_1 peak. We also find that the charge "$Q_{total\ anodic}$" is much greater than the charge introduced into the film by coulometry and is roughly equal to the opposite of the sum "$Q_{introduced}$" and "$Q_{reduction}$". In the CVs of the other electrodes, only the "$Q_{2\ anodic}$" load is important. It should be noted that for Ag300-FTO, $Q_{reduction}$ and $Q_{1\ anodic}$ are zero according to the absence of cathodic current at the start of the CV. Indeed, this thermally treated electrode does not contain, before CV, any silver (I) species soluble in the electrolyte. Surprisingly, Ag-FTO shows a non-negligible value of $Q_{reduction}$ while $Q_{1\ anodic}$ is zero. In this case, the coulometric formation of the silver NPs, have taken place in contact with FTO while for Ag-TiO_2 and Ag-SiO_2 electrodes, the NPs have been formed on the surface of the mesoporous oxide film. Thus, at the beginning of the Ag-FTO CV, the reduction of Ag^+ present in contact with FTO leads not to the crystallization of new silver NPs which would oxidize during a P_1 peak, but to the growth of the primitive NPs responsible for the P_2 peak. These results show that the anodic charge is more important in the Ag-TiO_2 system because the mesoporous structure of TiO_2 facilitates the reduction of silver ions at low potential.

Parameters influencing the characteristics of CVs of Ag-TiO_2 and Ag-SiO_2

Influence of the scanning speed

The scan speed allows electrochemical reactions to be distinguished by their speed. It also helps to establish the reversible or irreversible character of certain processes. The influence of the scanning speed on the "$Q_{1\ anodic}$" and "$Q_{2\ anodic}$" loads was first examined at the first scan. For both Ag-SiO_2 and Ag-TiO_2 electrodes, the "$Q_{2\ anodic}$" charge increases as the scan speed decreases (Figure 2a). For very slow scans, this charge approaches the absolute value of the introduced charge. Such a behavior certainly comes from a lower abrasion speed which protects the electrical contact of the NPs with the FTO when the scan is slow. The "$Q_{1\ anodic}$" charge, in the case of the TiO_2 film, increases even more significantly with the decrease in speed (Figure 2b). Indeed, the slower the potential zone in which the reduction of Ag^+ ions can take place is crossed, for the same available quantity of these ions in the TiO_2 film, the greater the quantity of silver formed.

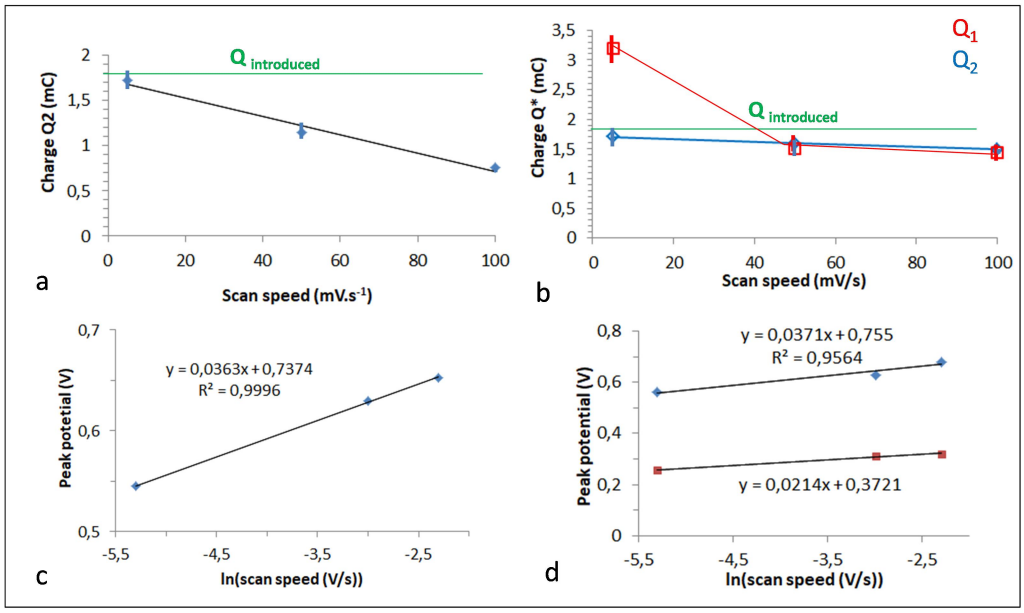

Figure 2: Influence of the scanning speed, on the electrochemical efficiency: (a): Ag-SiO_2, (b): Ag-TiO_2. "$Q_{1\ anodic}$" and "$Q_{2\ anodic}$" are the charges exchanged during the first anodic peak P_1 and during the second anodic peak P2, respectively. Influence of the scanning speed on the potential of the maximum of the peak: (c): Ag-SiO_2 peak P_2; (d): Ag-TiO_2 peak P_2 blue points, peak P_1 red points. The two anodic peaks P_1, with a maximum located at 0.32 V and P_2, with a maximum at 0.65 V, at a scan rate of 100mV.s^{-1}. The potential of the peaks is indicated to the nearest 0.005 mV

Next, we examine the influence of the scanning speed on the potential of the top of the peaks P_1 and P_2. Figures 2 c & d show a linear increase in the anodic peak potential with the logarithm of the scan rate. For the P_2 peak, blue dots and line, the slope has a value of ~0.037 V per logarithmic unit (Figures 2c and 2d). This value shows that the electronic transfer of this anodic process is irreversible.[23] For the P_1 peak of the TiO_2 films, red dots and line, the slope is lower ~0.021 V per logarithmic unit. But in this case, the charge "$Q_{1\ anodic}$" increases a lot as the scan rate decreases (Figure 2b). However, an increase in charge generally shifts the peak summit of the corresponding peak towards higher potentials.[23] This effect therefore attenuates the effect of the scan rate on the position of the P_1 peak, which explains the lower slope of the straight line $E_{summit\ of\ the\ peak}$ = f(ln(scan speed)), although we can assume that the behavior, at constant load, of the P_1 peak as a function of the scan rate must be close to that of the P_2 peak.

Influence of the starting potential of the CV

As the cathodic current recorded at the beginning of the Ag-TiO_2 CV starts at -0.3 V, disappears at around 0.15 V, a departure of the CV from this potential is highly likely to modify the observed phenomena. By doing so, the large charge $Q_{reduction}$ should be reduced or cancelled and as we have seen that the charge corresponding to peak P_1 is the opposite of the charge $Q_{reduction}$, the new CV run should confirm that peak P_1 is the most affected peak. Actually, when the CV of the titanium oxide film starts from 0.15 V to 1.1 V (Figure 3a), the strong initial cathodic current observed in the case of a departure from -0.3 V (Figure 1a), does not exist. Under these conditions, for this film, as for the silica film, we observe only one anodic peak P_2 whose top of the peak is located around 0.69 V (Ag-TiO_2 blue curve), 0.65 V (Ag-SiO_2 red curve). On return, a large cathodic wave (Figure 3b) starting below 0.2 V corresponds mainly to the reduction of Ag^+ ions formed in the P_2 anodic peak of the forward scan. On the next scan (-0.3 V->1.1 V), only an intense anodic peak appears around 0.37 V which we identify with the first anodic peak P_1 in Figure 1a. However, there is a significant difference in intensity between these two peaks. While the P_2 peaks in Figure 1a and 3b are of comparable height, as they result from the same charge introduced by coulometry (-1.8 mC), the P_1 peak in Figure 3b is about twice as intense as the first P_1 peak in Figure 1a. Indeed, the amount of electricity exchanged in the P_1 peak (Figure 3b) is approximately the sum of the amounts of electricity exchanged in the P_2 peak (Figures 3a & 3b) and in the P_1 peak (Figure 1a). Since the CV in Figure 3b starts at 0.15 V, this P_1 peak does not appear during the first scan.

The absence of the P_1 peak, when the first CV scan starts from 0.15 V shows that the NPs whose oxidation is responsible for the P_1 peak, have not been formed. The high cathode current recorded at the -0.30 V start of the second scan must be explained by the reduction of Ag^+ ions which forms silver NPs whose oxidation is manifested by the P_1 peak. We have to conclude, firstly, that in the Ag- TiO_2 electrode, the silver NPs formed by coulometry exist initially. Secondly, that when the CV starts from a sufficiently negative potential, a second population of silver NPs is formed by reduction of a very important quantity of Ag^+ ions retained in the TiO_2 film. We will specify in the following paragraph the location of these two populations.

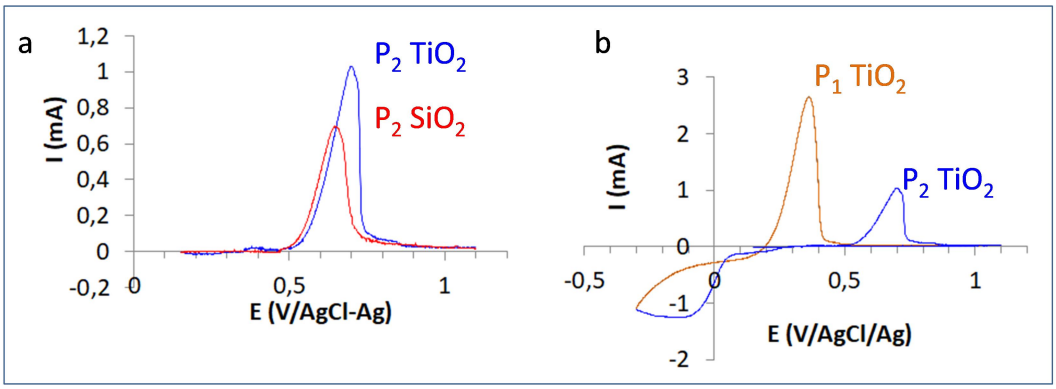

Figure 3 (a): Comparison of the first scan from 0.15 to 1.1 V for Ag-SiO_2 red curve and Ag-TiO_2 blue curve. (b): CV start of Ag-TiO_2 at 0.15 V. Comparison of the first cycle 0.15-> 1.1 V->-0.3 V blue curve and the second scan -0.3 V to1.1 V yellow curve. Electrolyte $NaNO_3$ 1 mol.L^{-1}, $V_{scan\ speed}$=100 mV.s^{-1}.

These results demonstrate that the P_1 peak is clearly related to the oxidation of silver NPs formed during the cathodic current between -0.3 and 0.15 V, as initially assumed.

Influence of particle size distribution.

The characteristics of the size distribution of the NPs (PSD) determine, for identical quantities of material and parameters of the CVs plot, the shape and position of the oxidation peak.[13,21–24] Simulation of the oxidation peak thus appears to be a mean of identifying and characterizing the population of NPs responsible for such a peak. In order to understand the origin of the two distinct oxidation peaks, we used the equations established by Brainina *& al.*[13] which, among other things, made it possible to calculate the intensity as a function of the potential recorded in the CVs during the electro-oxidation of polydisperse gold NPs.

$$i(t)=\theta_0 w(t) \int_0^{\infty} r^2 f_0(r-\int_0^t w(s)ds)dr \qquad (1)$$

Where $\theta_0=\frac{3Q_0}{<r^3>}$ and w is given by

$$w(t) = AaMe^{\beta B(E(t)-E_0)} - Ac(t)e^{-\alpha B(E(t)-E_0)} \qquad (2)$$

with $A = \frac{nMk_s}{\rho}$ et $B = \frac{nF}{RT}$ and $\alpha + \beta = 1$

$$c(t) = \frac{1}{FS_e\sqrt{4\pi}} \int_0^t \frac{i(s)}{\sqrt{t-s}} ds \qquad (3)$$

Definition of the entities used and values of some parameters:

i(t) the intensity over time t recorded in the CV.

c(t) the concentration of Ag^+ ions over time at the electrode. The value of c(0) initial concentration is given at the beginning of the calculation and can be modified.

r radius of the silver nanoparticles that constitute the distribution.

f_0 initial distribution of silver nanoparticles.

Q_0 quantity of electricity corresponding to the totality of the electroactive silver NPs introduced into the film.

Se electrode surface.

aM solid phase activity

E potential to which the electrode is subjected during the CV. $E = E_{initial} + vt$. v is the scan speed.

E_0 standard RedOx potential of the Ag^+/Ag couple. This potential is corrected for the size effect of the NPs according to the relation given by Plieth.[14] $E_0 = 0.5995 - 0.3388.r^{-1}(nm)$ V/AgCl/Ag. These corrected values are in good agreement with the OCP measurements made with films containing silver NPs whose radius is centered around 35 nm, as will be shown by microscopy analyses.

β and α are the coefficients of the electron transfer processes at the electrode.

n number of electrons exchanged in the process. n = 1.

k_s rate constant of the electron transfer.

M and ρ respectively molar mass and density of silver.

D diffusion coefficient of Ag^+ ions 10^{-9} $m^2.s^{-1}$ [23]

R perfect gas constant 8.314 $J.K^{-1}mol^{-1}$.

F Faraday 96485 $C.mol^{-1}$

Combining Equations (1)-(2)-(3) yields a functional equation for the unknown intensity function i(t). This functional equation can be related to non-linear integral equation with weak singularity coming from the square-root kernel appearing in (3). To compute a numerical solution to these equations, we have to approximate the time and radius integrals in (1) - (3). For the time integrals, we use a classic time-stepping method to compute them iteratively on a time-grid. The radius integral in (1) is approximated straightforwardly by a classic left point rule. The

program can take as input empirical initial distribution density f0 or user defined one. The simulated graphs below are obtained by using mixture of gaussian distributions.

Application to the P_2 peak of Ag-SiO_2 and of Ag-TiO_2

The analysis of the SEM image of the silica (Figure 4a) and titania (Figure 4b) films loaded with silver NPs by coulometry leads to the particle size distributions shown in Figure 5a and in Figure 5c respectively. These NPs, the only ones formed voluntarily, grow on the surface of the film that was in contact with the silver nitrate solution at the time of coulometry. They can then reach dimensions much larger than the diameter of the film mesopores, due to mild growing conditions. Figures 5b and Figure 5d compare the plot of the P_2 peak of the CV with that of the peak calculated by entering in relation (1), the characteristics obtained.

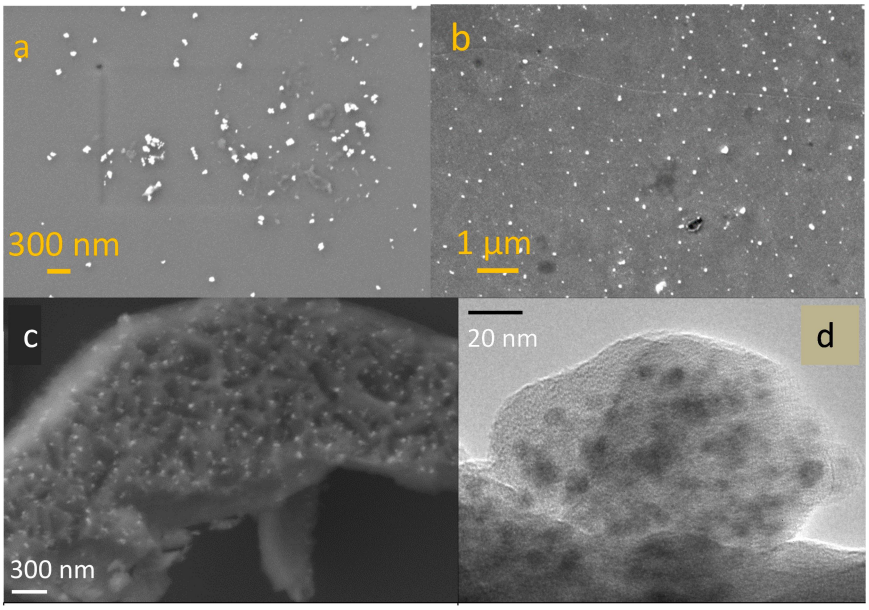

Figure 4: SEM image of the surface of the Ag-SiO_2 (a); of the surface of the Ag-TiO_2 (b). SEM image of the face of Ag-TiO_2 that was in contact with the FTO (c); TEM Image of Ag-TiO_2 in an area close to the FTO (d).

The differences between the calculated and experimental CVs are at the foot of the curves. The calculated peak rises more slowly than the experimental peak and falls more abruptly. The smoother simulated rise may be due to the fact that in the calculation, the E_0 potential does not decrease during the abrasion while the NPs become

smaller and smaller. The fall-off of the experimental peak, which extends over a much wider potential range, reflects the presence of aggregates of some NPs that behave almost like larger particles and broaden the peak.[8] The calculated peak position and height are very close to the experimental position and height.

Application to the P_1 peak of Ag-TiO_2

Figure 4c shows the SEM image of a titanium oxide film piece with silver NPs. These NPs were formed during a CV started at - 0.3 V and stopped at 0.1 V. The face of the piece observed in this image is the face that was in contact with the FTO layer. The silver NPs are thus formed in the vicinity of the FTO by reduction of the Ag^+ present in the mesopores and are smaller than those growing on the film surface by coulometry.

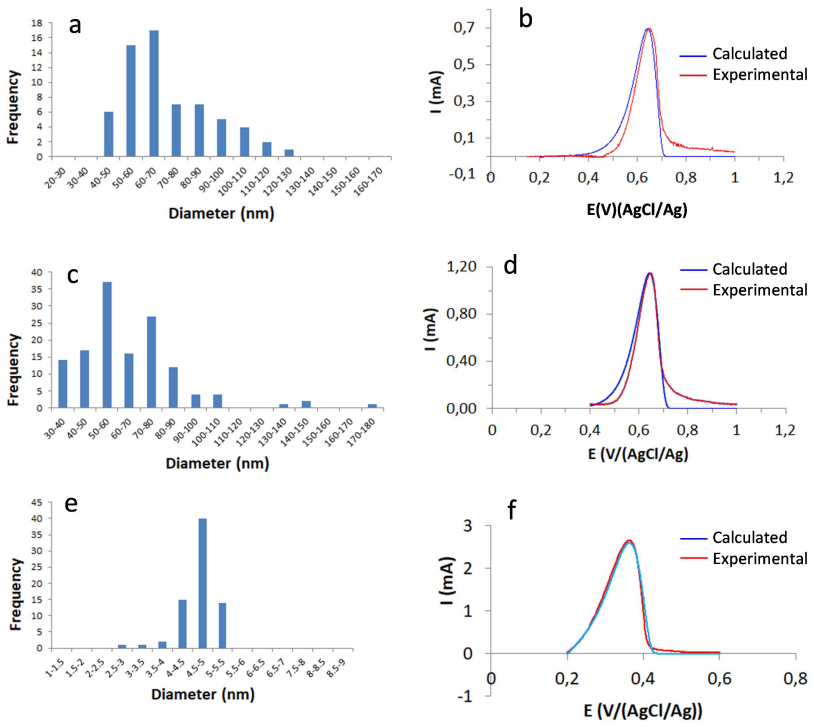

Figure 5: Size distribution of NPs from image J of the Ag-SiO_2 SEM picture of Figure 4a (a); CVs of the P_2 peak for Ag-SiO_2 (b) experimental red curve, calculated blue curve, scan speed = 100 $mV.s^{-1}$; mean radius = 36 nm. standard deviation = 13 nm. E_0 = 0.591 V; $k_s = 10^{-8}$ $m.s^{-1}$. Q_0 = 0.88 mC; c(0) = 0.5 $mol.m^{-3}$; Size distributions of NPs from image J of the Ag-TiO_2 SEM picture of Figure 4b (c); CVs of the P_2 peak for Ag-TiO_2 (d), experimental red curve, calculated blue curve. scan speed = 100 $mV.s^{-1}$; mean radius = 33.2 nm. standard deviation = 15.5 nm. E_0 = 0.589 V; ks = 10^{-8} $m.s^{-1}$. Q_0 = 1.4 mC; c(0) = 0.5 $mol.m^{-3}$; Size distribution extracted with ImageJ of the Ag-TiO_2 TEM picture of Figure 4d (e); Experimental CV, red curve. Calculated CV, blue curve (f). scan speed = 100 $mV.s^{-1}$. mean radius = 2.35 nm. Standard deviation = 0.45 nm. E0 = 0.455 V. ks = 10^{-8} $m.s^{-1}$. Q_0 = 3 mC. c(0) = 0.5 $mol.m^{-3}$.

The TEM image in Figure 4d confirms the presence of small silver NPs between the mesopores and FTO and leads to the distribution in Figure 5e. The P_1 peak calculated from this distribution and the experimental peak are plotted in Figure 5f and have a very good agreement. We first note that the average radius of the NPs giving rise to the P_1 peak and formed against the FTO is about more than ten time smaller as that of the NPs at the origin of the P_2 peak and located on the film surface. In the first case, the NPs are formed during the CV in a region of negative potentials between -300 and 100 mV, for 4 s, with an initial negative intensity of several mA, which lead to an abundant crystallization. Moreover, as these silver NPs are formed on the inner surface of the TiO_2 film, their strong adhesion to the support prevents their coalescence.[30,32,65] Whereas in the second case, the NPs are formed by coulometry at around between 480 and 500 mV, for 180 s, with a controlled intensity of -10 µA. Thus the particular conditions of electroreduction of Ag^+ ions leading to each of the two populations of NPs explain the differences in their size distribution and their reactivity. The difference in the reactivity of the two populations cannot be attributed to a difference in the crystallographic structure of the small NPs since the Selected Area Electronic diffraction (SAED) and High resolution transmission electron microscopy (HRTEM) images of the latter show that they are also composed of cubic silver. The simulation of the CVs of the two peaks, P_1 and P_2, is carried out with the same value of the electronic exchange constant, close to the one used in the previous work of Brainina et al.[13]

SEM observations of the Ag-SiO_2 and Ag-TiO_2 electrodes carried out after coulometry and before CV show that the silver NPs responsible for this P_2 peak are located on the film surface (Figures 4a and 4b). The high size distribution of this population must be attributed to the electrolysis conditions, low current -10 µA (1.7 $\mu A.cm^{-2}$) and potential ~ 500 mV close to the equilibrium potential of the Ag^+/Ag couple.

The silver NPs giving rise to this P_1 peak were discovered by SEM observation in the vicinity of the FTO in the Ag-TiO_2 electrode after a CV that started from -300 mV and stopped around 100 mV, i.e. before the onset of the P_1 peak (Figures 4c and 4d). These NPs are small because they are formed far from the electrochemical equilibrium and with a high reduction current of the order of several mA. Further studies by X-ray reflectometry would allow us to consolidate our observations made by electron microscopy.[56]

Retention of Ag^+ ions in TiO_2 films

CVs after a rest period

Whereas with silica films, the intensity of the redox phenomena of the CVs disappears after a small number of cycles (3 or 4), these phenomena persist after several tens of cycles with the titanium oxide films (Figure 1). This persistence is due to a reappearance of reducible Ag^+ ions in the electrode after each cycle. It was necessary to verify the existence and measure the extent of this behavior, in the absence of electrochemical conditions.

The blue curves in Figure 6a represent a series of six cycles with freshly prepared electrode, between -0.3 and 1.1 V at 0.1 $V.s^{-1}$. The very first cycles, the last of which was stopped at 1100 mV, are not represented.

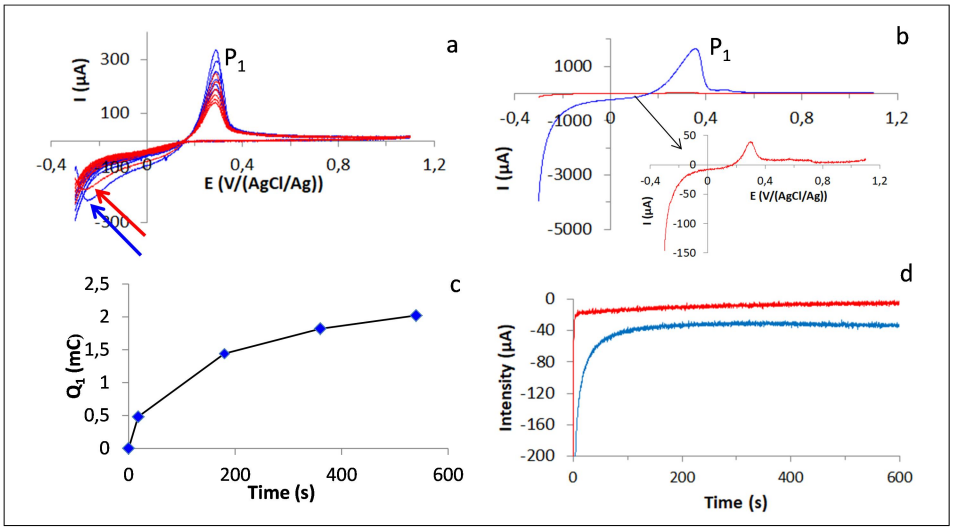

Figure 6: First series of six cycles of CV of Ag-TiO_2 (blue) and after a rest period (6 min), another series of six cycles (red) (a). CV of a titanium oxide film (blue curve) and a silica film (red curves) previously soaked for 9 min in silver nitrate solution 0.05 $mol.L^{-1}$ (b); Charge Q_1 measured under the P_1 peak as a function of the impregnation time of the titanium oxide film in silver nitrate solution 0.05 mol. L^{-1} (c); Chronoamperometry carried out for 10 min, at -200 mV, with a silica film, red curve, and a titanium oxide film, blue curve, which were soaked for 9 min in the 0.05 $mol.L^{-1}$ silver nitrate solution. The points acquired before time = 0.5 s are not represented on the curves so as not to crush them (d).

The intensity of the anodic peak decreases progressively and significantly during the first successive cycles. The height of the peak in the fifth cycle is about half that of the first cycle. After a rest period of 6 min, the film is subjected to a new series of CVs under the same conditions with red curves (Figure 6a). The anodic signal located

around 300 mV reappears. The height of the first peak of this new series is equal to that of the third peak of the first series and about 1.5 times as high as the peak of the last cycle of the previous series. We also notice that the beginning of the first cycle of both series is marked by a large cathodic peak (arrows), while all other cycles start with a maximum cathode current. This difference is due to the absence of silver NPs at the start of the CV, as these CVs were started after the film had already been cycled at high positive potentials (1.1 V), so that all silver NPs had been dissolved. On the contrary, for films loaded with silver NPs subjected for the first time to voltammetry starting from -0.3 V, the cathodic current is maximal from the start, as the presence of silver NPs favors the reduction of Ag^+ ions (Figure 1). This same behavior is also observed at the beginning of each new CV of a cycle when the previous voltammetry is continued to -0.3 V or to a more negative potential.

CVs after variable soak times

Prior experiments show an anodic peak P_1 appeared in the CVs of Ag-TiO_2 electrode when the scan starts from a sufficiently low potential. To study the effect of the electrochemical reduction method on Ag^+ impregnated inside mesoporous films and thus the P_1 peak, we have chosen to remove this step. Thus, we simply soak the mesoporous films (TiO_2 and SiO_2) in 0.05 mol.L^{-1} of silver nitrate solution and then subjected the electrode to a potential scan starting from -0.3V to 1.1V in molar sodium nitrate medium (Figure 6b).

The P_1 peak appears well in both CVs, but with a different intensity; indeed the peak of the CV plotted with the titanium oxide film is 40 times higher than the peak of the CV plotted with the silica film. The amount of electricity Q_1 involved in this anodic peak P_1 is 50 µC and 2020 µC, respectively for the silica and titanium oxide films. Note that the charge represented by the silver ions brought by the 0.05 mol.L^{-1} silver nitrate solution that may have remained in the pores is less than 0.5 mC (0.33 mC for a thickness of 200 nm and a percentage of pore volume of 50 %). These ions stagnating totally or partially in the pores of the film after impregnation could explain the existence of the very small P_1 peak of the silica film, but cannot explain the very large P_1 peak of the titanium oxide film. Malati *& al*[67] showed that although the point of zero charge (PZC) of silica (2.8) is lower than that of titania (5.3 to 6.2), titania adsorbs a higher amount of silver ions.

When the impregnation time of the titanium oxide film in the 0.05 mol.L^{-1} silver nitrate solution increases from 18 s to 540 s, the amount of adsorbed Ag^+ increases (Figure 6c). We note that the equilibrium value exceeds widely 2 mC. The estimation of the amount of silver ion corresponding to this charge leads to $2.1.10^{-5}$ mol $Ag^+/gTiO_2$. This quantity is of the same order of magnitude as those of silver ions adsorbed at equilibrium in a silver nitrate solution of the same concentration, $6.7.10^{-5}$ and $2.0.10^{-5}$ mol $Ag^+/gTiO_2$, respectively measured by Misra *& al*.[66] and Malati *& al*.[67]

Chronoamperometry and EDX analyses

The above results show that the mesoporous titania film is capable of releasing gradually a significant amount of previously adsorbed Ag^+ ions. Comparison of the CA curves at -0.2 V of a silica film and a titania film soaked in 0.05 mol.L^{-1} silver nitrate solution, during 9 min, should reveal a significant difference.

Figure 6d shows that at -200 mV the silica film curve quickly reaches a very low cathodic current. In the case of the titanium oxide film, this current also decreases very rapidly in the first moments, but after about 150 s, stabilizes at around -30 µA. The amounts of electricity involved during the CA at -200 mV of these two films are very different, i.e. - 0.41 mC for the silica film and - 2.4 mC for the titania film. The titanium oxide film adsorbs about six times more silver ions than the silica film. It should be noted that the amount of Ag^+ ions stored in the titanium oxide film, measured by CA at a pH of about 6, at 298 K and expressed in relation to the specific surface area, is close to the value determined for anatase by Malati & al[67], i.e. approximately 7.10^{-7} mol $Ag^+.m^{-2}$.

The atomic ratios Ag/Si and Ag/Ti are measured by EDX analysis during SEM examinations of silica and titania films that are been left for 9 min in the 0.05 mol.L^{-1} silver nitrate solution. The averages calculated over five analyses are Ag/Ti = $8.4.10^{-3}$ and Ag/Si = $1.7.10^{-3}$. These ratios allow us to obtain an estimate of the quantity of silver ions retained in these films and therefore of the quantity of electricity associated with them. Considering similar thicknesses and pore fractions of the film, i.e. 200 nm thick and 50% porous volume, the quantity of silver ions retained corresponds to approximately 0.33 mC and 3.65 mC respectively for the silica and titanium oxide films. These values are of the same order of magnitude as those determined by chronoamperometry.

Diffusion experiences

The results presented in the previous paragraph showed the difference in the retention of Ag^+ ions in the Ag-TiO_2 electrode and in the Ag-SiO_2 electrode. We then tried to test the consequences of such a difference on the rate of exit of Ag^+ ions from these electrodes when they are immersed in an electrolyte free of Ag^+ ions. These diffusion experiments are based on the measurement of the OCP. For this purpose, silica and titania films are first loaded with silver NPs by coulometry with a charge of -1.8 mC. In the presence of Ag^+ ions, the potential (OCP) of these electrodes is that of the Ag^+/NPs silver couple and obeys Nernst's law. Its measurement, when the films are immersed in silver nitrate solutions of different concentrations and known ionic strength, shows that the values of the normal potential of the Ag^+/Ag couple for both films are close to and within 10 mV of the usual standard potential 0.7995 V/ NHE.

Such silica and titania films impregnated with silver ions (soaked in silver nitrate solution for 10 min) are then immersed in a sodium nitrate solution (pH = 6) while the OCP of these two electrodes is monitored for 10 minutes (Figure 7a). The silver ion concentration over time calculated from the OCP is shown in Figure 7b.

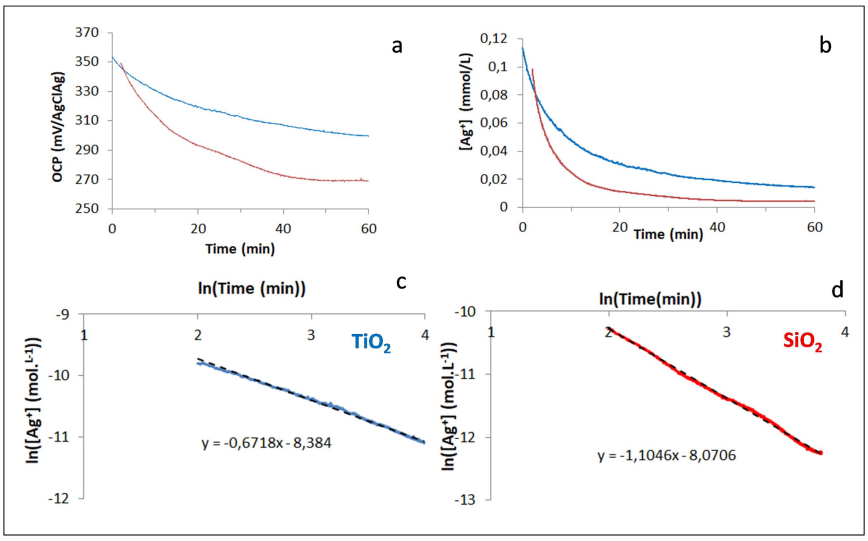

Figure 7: Evolution as a function of time of OCP (a); Silver ion concentration (b). Blue curves TiO_2 film. Red curves SiO_2 film. Representation $\ln[Ag^+] = f(\ln(t))$ for TiO_2 film (c) and for SiO_2 film (d).

These curves show that the silica film loses silver ions more rapidly than the titania film. The log-log plot in Figures 7c &d show a linear evolution with a much more negative slope for the silica film and far from the -0.5 expected for pure diffusion of a species initially distributed in a thin layer in a plate diffusing in an external medium of infinite extent.

Etienne & al[53] explain the role of silica as a diffusion barrier for anions by the low IEP value of ~2.8. Titanium oxide has an IEP between 6 and 7. The lower Ag^+ cation diffusion rate outward the titanium oxide film than that outward the silica film cannot be explained by an electrostatic cause nor by the similar pore size in both films compared to that of hydrated silver. This difference must be attributed to the important binding of silver ions on the pores walls of TiO_2. These adsorbed ions are progressively desorbed during the diffusion of Ag^+ ions out of the film, which slows down their disappearance from the film.

Conclusions

Mesoporous silica and titania films deposited on FTO and containing silver nanoparticles have been studied by electrochemistry methods. The results presented in this article highlight the importance of the physicochemical nature of the film that encloses the silver NPs. They emphasize the singular behavior of mesoporous titanium oxide films during the electrochemical redox phenomena of the silver NPs they contain. This is revealed by the observation of the existence of two anodic potential peaks in the CVs. They are explained by the presence of two populations of silver NPs created in two distinct areas of the film and with different size distributions. This behavior is mainly due to the ability of these films to adsorb large amounts of Ag^+ ions. Silver ions previously introduced by impregnation escape more rapidly from mesoporous silica films than from titanium oxide films. In the latter, adsorbed ions are gradually released into the liquid filling the pores and are reduced when CVs start from potentials below 0 V; they can thus form a large number of NPs in the vicinity of the FTO substrate. This population has a narrower size distribution around a smaller size than the coulometrically introduced NPs located on the film surface. The anodic peaks recorded during the CVs are simulated quite well for very different size distributions of silver nanoparticles while keeping the same value of the electronic transfer constant. This work

shows the importance of being very careful about the consequences of the experimental conditions in cyclic voltammetry when interpreting the electrochemical behavior of metal nanoparticles.

AUTHOR INFORMATION

Corresponding Author

* Fernand Chassagneux: fernand.chassagneux@univ-lyon1.fr

* Laurence Bois: laurence.bois@univ-lyon1.fr

Author Contributions

The manuscript was written through contributions of all authors. All authors have given approval to the final version of the manuscript. FC and LB did the experiments. FC wrote the initial paper draft. All the authors contributed to revise the paper.

Funding Sources

This work was supported by the LABEX iMUST (ANR-10-LABX-0064) of the Université de Lyon, within the program "Investing in the Future" (ANR-11-IDEX-0007) by the French National Research Agency (ANR).

ACKNOWLEDGMENT

The authors gratefully acknowledge the Ctμ platform of electronic microscopy (University Lyon 1). The authors would like to thank Jean-François Chassagneux (Laboratoire de Probabilités, Statistique et Modélisation, LPSM, UMR 8001, Université Paris Cité), for numerical simulations and fruitful discussions.

ABBREVIATIONS

CV: Cyclic Voltammetry, CA: chronoamperometry, OCP: Open Circuit Potential, EDX: Energy-Dispersive X-ray, SEM: Scanning Electron Microscopy, TEM: Transmission Electron Microscopy, NPs: Nanoparticles, IEP: Isoelectric point, PZC: point of zero charge.

REFERENCES

(1) Kang, H.; Buchman, J. T.; Rodriguez, R. S.; Ring, H. L.; He, J.; Bantz, K. C.; Haynes, C. L. Stabilization of Silver and Gold Nanoparticles: Preservation and Improvement of Plasmonic Functionalities. *Chem. Rev.* **2019**, *119* (1), 664–699. https://doi.org/10.1021/acs.chemrev.8b00341.

(2) Pattadar, D. K.; Zamborini, F. P. Effect of Size, Coverage, and Dispersity on the Potential-Controlled Ostwald Ripening of Metal Nanoparticles. *Langmuir* **2019**, *35* (50), 16416–16426. https://doi.org/10.1021/acs.langmuir.9b02421.

(3) Mainali, B. P.; Pattadar, D. K.; Zamborini, F. P. Reverse Size-Dependent Electrooxidation of Gold Nanoparticles Coated with Alkanethiol Self-Assembled Monolayers. *J. Phys. Chem. C* **2021**, *125* (4), 2719–2728. https://doi.org/10.1021/acs.jpcc.0c10173.

(4) Pattadar, D. K.; Zamborini, F. P. Size Stability Study of Catalytically Active Sub-2 Nm Diameter Gold Nanoparticles Synthesized with Weak Stabilizers. *J. Am. Chem. Soc.* **2018**, *140* (43), 14126–14133. https://doi.org/10.1021/jacs.8b06830.

(5) Sharma, J. N.; Pattadar, D. K.; Mainali, B. P.; Zamborini, F. P. Size Determination of Metal Nanoparticles Based on Electrochemically Measured Surface-Area-to-Volume Ratios. *Anal. Chem.* **2018**, *90* (15), 9308–9314. https://doi.org/10.1021/acs.analchem.8b01905.

(6) Ma, H.; Gao, P.; Qian, P.; Su, Y. Size-Dependent Electrochemical Properties of Pure Metallic Nanoparticles. *J. Phys. Chem. C* **2020**, *124* (5), 3403–3409. https://doi.org/10.1021/acs.jpcc.9b10962.

(7) Allen, S. L.; Sharma, J. N.; Zamborini, F. P. Aggregation-Dependent Oxidation of Metal Nanoparticles. *J. Am. Chem. Soc.* **2017**, *139* (37), 12895–12898. https://doi.org/10.1021/jacs.7b05957.

(8) Chen, W.; Wang, H.; Tang, H.; Yang, C.; Li, Y. Unique Voltammetry of Silver Nanoparticles: From Single Particle to Aggregates. *Anal. Chem.* **2019**, *91* (22), 14188–14191. https://doi.org/10.1021/acs.analchem.9b03372.

(9) Pattadar, D. K.; Nambiar, H. N.; Allen, S. L.; Jasinski, J. B.; Zamborini, F. P. Effect of Metal Nanoparticle Aggregate Structure on the Thermodynamics of Oxidative Dissolution. *Langmuir* **2021**, *37* (24), 7320–7327. https://doi.org/10.1021/acs.langmuir.1c00565.

(10) Hua, H.; Liu, Y.; Wang, D.; Li, Y. Size-Dependent Voltammetry at Single Silver Nanoelectrodes. *Anal. Chem.* **2018**, *90* (16), 9677–9681. https://doi.org/10.1021/acs.analchem.8b02644.

(11) Liang, C.; Lu, Z.-A.; Wu, J.; Chen, M.-X.; Zhang, Y.; Zhang, B.; Gao, G.-L.; Li, S.; Xu, P. Recent Advances in Plasmon-Promoted Organic Transformations Using Silver-Based Catalysts. *ACS Appl. Mater. Interfaces* **2020**, *12* (49), 54266–54284. https://doi.org/10.1021/acsami.0c15192.

(12) Guo, L.; Yin, H.; Xu, M.; Zheng, Z.; Fang, X.; Chong, R.; Zhou, Y.; Xu, L.; Xu, Q.; Li, J.; Li, H. In Situ Generated Plasmonic Silver Nanoparticle-Sensitized Amorphous Titanium Dioxide for Ultrasensitive Photoelectrochemical Sensing of Formaldehyde. *ACS Sens.* **2019**, *4* (10), 2724–2729. https://doi.org/10.1021/acssensors.9b01204.

(13) Brainina, Kh. Z.; Galperin, L. G.; Kiryuhina, T. Yu.; Galperin, A. L.; Stozhko, N. Yu.; Murzakaev, A. M.; Timoshenkova, O. R. Silver Nanoparticles Electrooxidation: Theory and Experiment. *J. Solid State Electrochem.* **2012**, *16* (7), 2365–2372. https://doi.org/10.1007/s10008-011-1583-5.
(14) Plieth, W. J. On the Electrochemical Properties of Small Clusters of Metal Atoms and their Role in the Surface Enhanced Raman Scattering. *J. Phys. Chem.* **1982**, 86, 16, 3166-3170. https://doi.org/10.1021/j100213a020.
(15) Henglein, A. Small-Particle Research: Physicochemical Properties of Extremely Small Colloidal Metal and Semiconductor Particles. *Chem. Rev.* **1989**, *89* (8), 1861–1873. https://doi.org/10.1021/cr00098a010.
(16) Redmond, P. L.; Hallock, A. J.; Brus, L. E. Electrochemical Ostwald Ripening of Colloidal Ag Particles on Conductive Substrates. *Nano Lett.* **2005**, *5* (1), 131–135. https://doi.org/10.1021/nl048204r.
(17) Ivanova, O. S.; Zamborini, F. P. Size-Dependent Electrochemical Oxidation of Silver Nanoparticles. *J. Am. Chem. Soc.* **2010**, *132* (1), 70–72. https://doi.org/10.1021/ja908780g.
(18) Brainina, Kh. Z.; Galperin, L. G.; Vikulova, E. V. Electrochemistry of Metal Nanoparticles: The Effect of Substrate. *J. Solid State Electrochem.* **2012**, *16* (7), 2357–2363. https://doi.org/10.1007/s10008-012-1721-8.
(19) Brainina, K. Z.; Vydrevich, M. B. Stripping Analysis of Solids. *J. Electroanal. Chem*. **1981**, 121, 1-28
(20) Chevallier, F. G.; Goodwin, A.; Banks, C. E.; Jiang, L.; Jones, T. G. J.; Compton, R. G. Abrasively Modified Electrodes: Mathematical Modelling and Numerical Simulation of Electro-chemical Dissolution/ Growth Processes under Cyclic Voltammetric Conditions. *J Solid State Electrochem*, **2006**, 10, 857-864. https:// doi 10.1007/s10008-006-0152-98.
(21) Ward Jones, S. E.; Campbell, F. W.; Baron, R.; Xiao, L.; Compton, R. G. Particle Size and Surface Coverage Effects in the Stripping Voltammetry of Silver Nanoparticles: Theory and Experiment. *J. Phys. Chem. C* **2008**, *112* (46), 17820–17827. https://doi.org/10.1021/jp807093q.
(22) Ward Jones, S. E.; Chevallier, F. G.; Paddon, C. A.; Compton, R. G. General Theory of Cathodic and Anodic Stripping Voltammetry at Solid Electrodes: Mathematical Modeling and Numerical Simulations. *Anal. Chem.* **2007**, *79* (11), 4110–4119. https://doi.org/10.1021/ac070046b.
(23) Toh, H. S.; Batchelor-McAuley, C.; Tschulik, K.; Uhlemann, M.; Crossley, A.; Compton, R. G. The Anodic Stripping Voltammetry of Nanoparticles: Electrochemical Evidence for the Surface Agglomeration of Silver Nanoparticles. *Nanoscale* **2013**, *5* (11), 4884. https://doi.org/10.1039/c3nr00898c.
(24) Brainina, K. Z.; Galperin, L. G.; Galperin, A. L. Mathematical Modeling and Numerical Simulation of Metal Nanoparticles Electrooxidation. *J. Solid State Electrochem.* **2010**, *14* (6), 981–988. https://doi.org/10.1007/s10008-009-0897-z.
(25) Brainina, Kh. Z.; Galperin, L. G.; Vikulova, E. V.; Galperin, A. L. The Effect of the System Polydispersity on Voltammograms of Nanoparticles Electrooxidation. *J. Solid State Electrochem.* **2013**, *17* (1), 43–53. https://doi.org/10.1007/s10008-012-1852-y.
(26) Cueto-Gómez, L. F.; Garcia-Gómez, N. A.; Mosqueda, H. A.; Sánchez, E. M. Electrochemical Study of TiO2 Modified with Silver Nanoparticles upon CO2 Reduction. *J. Appl. Electrochem.* **2014**, *44* (5), 675–682. https://doi.org/10.1007/s10800-014-0677-z.
(27) Rosen, J.; Hutchings, G. S.; Lu, Q.; Rivera, S.; Zhou, Y.; Vlachos, D. G.; Jiao, F. Mechanistic Insights into the Electrochemical Reduction of CO_2 to CO on Nanostructured Ag Surfaces. *ACS Catal.* **2015**, *5* (7), 4293–4299. https://doi.org/10.1021/acscatal.5b00840.
(28) Schlexer, P.; Ruiz Puigdollers, A.; Pacchioni, G. Tuning the Charge State of Ag and Au Atoms and Clusters Deposited on Oxide Surfaces by Doping: A DFT Study of the Adsorption Properties of

Nitrogen- and Niobium-Doped TiO $_2$ and ZrO $_2$. *Phys. Chem. Chem. Phys.* **2015**, *17* (34), 22342–22360. https://doi.org/10.1039/C5CP03834K.
(29) Schvval, A. B.; Juan, A.; Cabeza, G. F. Theoretical Study of the Role of the Interface of Ag4 Nanoclusters Deposited on TiO2(110) and TiO2(101). *Appl. Surf. Sci.* **2019**, *490*, 343–351. https://doi.org/10.1016/j.apsusc.2019.05.291.
(30) Mao, Z.; Rumptz, J. R.; Campbell, C. T. Energetics of Ag Adsorption on and Adhesion to Rutile TiO $_2$ (100) Studied by Microcalorimetry. *J. Phys. Chem. C* **2021**, *125* (5), 3036–3046. https://doi.org/10.1021/acs.jpcc.0c10504.
(31) Yang, H.; Chen, F.; Jiao, Y.; Zhang, J. The Role of Interfacial Lattice Ag+ on Titania Based Photocatalysis. *Appl. Catal. B Environ.* **2013**, *130–131*, 218–223. https://doi.org/10.1016/j.apcatb.2012.10.033.
(32) Zhou, W.; Li, T.; Wang, J.; Qu, Y.; Pan, K.; Xie, Y.; Tian, G.; Wang, L.; Ren, Z.; Jiang, B.; Fu, H. Composites of Small Ag Clusters Confined in the Channels of Well-Ordered Mesoporous Anatase TiO2 and Their Excellent Solar-Light-Driven Photocatalytic Performance. *Nano Res.* **2014**, *7* (5), 731–742. https://doi.org/10.1007/s12274-014-0434-y.
(33) 정순관. Electrocatalytic Reduction of Hydrogen Peroxide on Silver Nanoparticles Stabilized by Amine Grafted Mesoporous SBA-15. *Bull. Korean Chem. Soc.* **2010**, *31* (12), 3668–3674. https://doi.org/10.5012/BKCS.2010.31.12.3668.
(34) Wolosiuk, A.; Tognalli, N. G.; Martínez, E. D.; Granada, M.; Fuertes, M. C.; Troiani, H.; Bilmes, S. A.; Fainstein, A.; Soler-Illia, G. J. A. A. Silver Nanoparticle-Mesoporous Oxide Nanocomposite Thin Films: A Platform for Spatially Homogeneous SERS-Active Substrates with Enhanced Stability. *ACS Appl. Mater. Interfaces* **2014**, *6* (7), 5263–5272. https://doi.org/10.1021/am500631f.
(35) Wang, H.; Zhang, Y.; Yu, H.; Wu, D.; Ma, H.; Li, H.; Du, B.; Wei, Q. Label-Free Electrochemical Immunosensor for Prostate-Specific Antigen Based on Silver Hybridized Mesoporous Silica Nanoparticles. *Anal. Biochem.* **2013**, *434* (1), 123–127. https://doi.org/10.1016/j.ab.2012.11.012.
(36) Cincotto, F. H.; Canevari, T. C.; Campos, A. M.; Landers, R.; Machado, S. A. S. Simultaneous Determination of Epinephrine and Dopamine by Electrochemical Reduction on the Hybrid Material SiO $_2$ /Graphene Oxide Decorated with Ag Nanoparticles. *The Analyst* **2014**, *139* (18), 4634. https://doi.org/10.1039/C4AN00580E.
(37) Ohko, Y.; Tatsuma, T.; Fujii, T.; Naoi, K.; Niwa, C.; Kubota, Y.; Fujishima, A. Multicolour Photochromism of TiO2 Films Loaded with Silver Nanoparticles. *Nat. Mater.* **2003**, *2* (1), 29–31. https://doi.org/10.1038/nmat796.
(38) Matsubara, K.; Tatsuma, T. Morphological Changes and Multicolor Photochromism of Ag Nanoparticles Deposited on Single-Crystalline TiO2 Surfaces. *Adv. Mater.* **2007**, *19* (19), 2802–2806. https://doi.org/10.1002/adma.200602823.
(39) Kazuma, E.; Tatsuma, T. Photoinduced Reversible Changes in Morphology of Plasmonic Ag Nanorods on TiO $_2$ and Application to Versatile Photochromism. *Chem Commun* **2012**, *48* (12), 1733–1735. https://doi.org/10.1039/C2CC16589A.
(40) Kafizas, A.; A. Parry, S.; Chadwick, A. V.; Carmalt, C. J.; Parkin, I. P. An EXAFS Study on the Photo-Assisted Growth of Silver Nanoparticles on Titanium Dioxide Thin-Films and the Identification of Their Photochromic States. *Phys. Chem. Chem. Phys.* **2013**, *15* (21), 8254. https://doi.org/10.1039/c3cp44513e.
(41) Zhang, H.; Wang, G.; Chen, D.; Lv, X.; Li, J. Tuning Photoelectrochemical Performances of Ag−TiO $_2$ Nanocomposites via Reduction/Oxidation of Ag. *Chem. Mater.* **2008**, *20* (20), 6543–6549. https://doi.org/10.1021/cm801796q.
(42) Tatsuma, T.; Suzuki, K. Photoelectrochromic Cell with a Ag–TiO2 Nanocomposite: Concepts of Drawing and Display Modes. *Electrochem. Commun.* **2007**, *9* (4), 574–576. https://doi.org/10.1016/j.elecom.2006.10.044.

(43) Matsubara, K.; Kelly, K. L.; Sakai, N.; Tatsuma, T. Plasmon Resonance-Based Photoelectrochemical Tailoring of Spectrum, Morphology and Orientation of Ag Nanoparticles on TiO2 Single Crystals. *J. Mater. Chem.* **2009**, *19* (31), 5526. https://doi.org/10.1039/b906795g.
(44) Bois, L.; Chassagneux, F.; Battie, Y.; Bessueille, F.; Mollet, L.; Parola, S.; Destouches, N.; Toulhoat, N.; Moncoffre, N. Chemical Growth and Photochromism of Silver Nanoparticles into a Mesoporous Titania Template. *Langmuir* **2010**, *26* (2), 1199–1206. https://doi.org/10.1021/la902339j.
(45) Ma, H.; Bakhti, S.; Rudenko, A.; Vocanson, F.; Slaughter, D. S.; Destouches, N.; Itina, T. E. Laser-Generated Ag Nanoparticles in Mesoporous TiO_2 Films: Formation Processes and Modeling-Based Size Prediction. *J. Phys. Chem. C* **2019**, *123* (42), 25898–25907. https://doi.org/10.1021/acs.jpcc.9b05561.
(46) Couzon, N.; Maillard, M.; Bois, L.; Chassagneux, F.; Brioude, A. Electrochemical Observation of the Plasmonic Effect in Photochromic Ag Nanoparticle Filled Mesoporous TiO_2 Films. *J. Phys. Chem. C* **2017**, *121* (40), 22147–22155. https://doi.org/10.1021/acs.jpcc.7b07155.
(47) Couzon, N.; Maillard, M.; Chassagneux, F.; Brioude, A.; Bois, L. Photoelectrochemical Behavior of Silver Nanoparticles inside Mesoporous Titania: Plasmon-Induced Charge Separation Effect. *Langmuir*, **2019**, 35, 7, 2517-2526. https://doi.org/10.1021/acs.langmuir.8b03617.
(48) Medveď, I.; Černý, R. Surface Diffusion in Porous Media: A Critical Review. *Microporous Mesoporous Mater.* **2011**, *142* (2–3), 405–422. https://doi.org/10.1016/j.micromeso.2011.01.015.
(49) Bousige, C.; Levitz, P.; Coasne, B. Bridging Scales in Disordered Porous Media by Mapping Molecular Dynamics onto Intermittent Brownian Motion. *Nat. Commun.* **2021**, *12* (1), 1043. https://doi.org/10.1038/s41467-021-21252-x.
(50) Tartakovsky, D. M.; Dentz, M. Diffusion in Porous Media: Phenomena and Mechanisms. *Transp. Porous Media* **2019**, *130* (1), 105–127. https://doi.org/10.1007/s11242-019-01262-6.
(51) Linares Moreau, M. M.; Martínez, E. D.; Fuertes, M. C.; Zelcer, A.; Golmar, F.; Granell, P. N.; Levy, P. E.; Soler Illia, G. J. A. A.; Granja, L. P. Microscopic Electrochemical Control of Ag Nanoparticles into Mesoporous TiO_2 Thin Films. *J. Phys. Chem. C* **2019**, *123* (6), 3579–3587. https://doi.org/10.1021/acs.jpcc.8b11217.
(52) Massari, A. M.; Gurney, R. W.; Schwartz, C. P.; Nguyen, S. T.; Hupp, J. T. Walljet Electrochemistry: Quantifying Molecular Transport through Metallopolymeric and Zirconium Phosphonate Assembled Porphyrin Square Thin Films. *Langmuir* **2004**, *20* (11), 4422–4429. https://doi.org/10.1021/la049900+.
(53) Etienne, M.; Quach, A.; Grosso, D.; Nicole, L.; Sanchez, C.; Walcarius, A. Molecular Transport into Mesostructured Silica Thin Films: Electrochemical Monitoring and Comparison between *p* 6 *m* , P6 $_3$ / *Mmc* , and *Pm* 3 *n* Structures. *Chem. Mater.* **2007**, *19* (4), 844–856. https://doi.org/10.1021/cm0625068.
(54) Brinker, C. J. Evaporation-Induced Self-Assembly: Functional Nanostructures Made Easy. *MRS Bull.* **2004**, *29* (9), 631–640. https://doi.org/10.1557/mrs2004.183.
(55) Mahoney, L.; Koodali, R. Versatility of Evaporation-Induced Self-Assembly (EISA) Method for Preparation of Mesoporous TiO2 for Energy and Environmental Applications. *Materials* **2014**, *7* (4), 2697–2746. https://doi.org/10.3390/ma7042697.
(56) Fuertes, M. C.; Marchena, M.; Marchi, M. C.; Wolosiuk, A.; Soler-Illia, G. J. A. A. Controlled Deposition of Silver Nanoparticles in Mesoporous Single- or Multilayer Thin Films: From Tuned Pore Filling to Selective Spatial Location of Nanometric Objects. *Small* **2008**, *5* (2), 272–280. https://doi.org/10.1002/smll.200800894.
(57) Poroshkov, V. P.; Gurin, V. S. Surface Structures on Titanium Dioxide Electrodes after Electrochemical Silver Deposition. *Surf. Sci.* **1995**, *331–333*, 1520–1525. https://doi.org/10.1016/0039-6028(95)00370-3.

(58) Penner, R. M. Mesoscopic Metal Particles and Wires by Electrodeposition. *J. Phys. Chem. B* **2002**, *106* (13), 3339–3353. https://doi.org/10.1021/jp013219o.
(59) Dávila-Martínez, R. E.; Cueto, L. F.; Sánchez, E. M. Electrochemical Deposition of Silver Nanoparticles on TiO2/FTO Thin Films. *Surf. Sci.* **2006**, *600* (17), 3427–3435. https://doi.org/10.1016/j.susc.2006.06.041.
(60) Pérez, M. D.; Otal, E.; Bilmes, S. A.; Soler-Illia, G. J. A. A.; Crepaldi, E. L.; Grosso, D.; Sanchez, C. Growth of Gold Nanoparticle Arrays in TiO $_2$ Mesoporous Matrixes. *Langmuir* **2004**, *20* (16), 6879–6886. https://doi.org/10.1021/la0497898.
(61) Couzon, N.; Roiban, L.; Chassagneux, F.; Bois, L.; Brioude, A.; Maillard, M. Electroactive Area from Porous Oxide Films Loaded with Silver Nanoparticles: Electrochemical and Electron Tomography Observations. *ACS Appl. Mater. Interfaces* **2019**, *11* (40), 37270–37278. https://doi.org/10.1021/acsami.9b11581.
(62) Alberti, S.; Steinberg, P. Y.; Giménez, G.; Amenitsch, H.; Ybarra, G.; Azzaroni, O.; Angelomé, P. C.; Soler-Illia, G. J. A. A. Chemical Stability of Mesoporous Oxide Thin Film Electrodes under Electrochemical Cycling: From Dissolution to Stabilization. *Langmuir* **2019**, *35* (19), 6279–6287. https://doi.org/10.1021/acs.langmuir.9b00224.
(63) Bindini, E.; Chehadi, Z.; Faustini, M.; Albouy, P.-A.; Grosso, D.; Cattoni, A.; Chanéac, C.; Azzaroni, O.; Sanchez, C.; Boissière, C. Following in Situ the Degradation of Mesoporous Silica in Biorelevant Conditions: At Last, a Good Comprehension of the Structure Influence. *ACS Appl. Mater. Interfaces* **2020**, *12* (12), 13598–13612. https://doi.org/10.1021/acsami.9b19956.
(64) Giovanni, M.; Pumera, M. Size Dependant Electrochemical Behavior of Silver Nanoparticles with Sizes of 10, 20, 40, 80 and 107 Nm. *Electroanalysis* **2012**, *24* (3), 615–617. https://doi.org/10.1002/elan.201100690.
(65) Plessow, P. N.; Campbell, C. T. Influence of Adhesion on the Chemical Potential of Supported Nanoparticles as Modeled with Spherical Caps. *ACS Catal.* **2022**, *12* (4), 2302–2308. https://doi.org/10.1021/acscatal.1c04633.
(66) Misra, D. N. "Adsorption" of Silver Ions on Titanium Dioxide. *J. Colloid Interface Sci.* **1968**, *28* (1), 24–27. https://doi.org/10.1016/0021-9797(68)90201-4.
(67) Malati, M.A.; McEvoy, M.; Harvey, C.R. The adsorption of cadmium(II) and silver(I) ions on SiO_2 and on TiO_2. *Surface Technology*, **1982**, 17, 165-174. https://doi.org/10.1016/0376-4583(82)90019-X.

For Table of Contents Only